ELSEVIER

Sensors and Actuators A 50 (1995) 55–65

SENSORS AND ACTUATORS A PHYSICAL

A silicon force sensor for robotics and medicine

David J. Beebe [a], Arthur S. Hsieh [b], Denice D. Denton [c], Robert G. Radwin [d]

[a] *Department of Biomedical Engineering, Institute for Micromanufacturing, Louisiana Tech University, 711 South Vienna Street, Ruston, LA 71270, USA*
[b] *Department of Biomedical Engineering, University of Southern California, University Park, Los Angeles, CA 90089-1451, USA*
[c] *Department of Electrical and Computer Engineering, 1415 Johnson Drive, University of Wisconsin-Madison, Madison WI 53706, USA*
[d] *Department of Industrial Engineering, 1513 University Avenue, University of Wisconsin-Madison, Madison, WI 53706, USA*

Received 11 May 1994; in revised form 26 June 1995; accepted 19 September 1995

Abstract

This paper describes the development of a silicon-based force sensor packaged in a flexible polyimide-based package. The fabrication process is compatible with standard integrated circuit processes and produces a flexible package that sandwiches the metal leads between protective polyimide layers. Silicon direct bonding and bulk micromachining (both isotropic and anisotropic) are utilized to fabricate the silicon sensing element. The sensing element consists of a circular diaphragm (200 μm thick with a 2000 μm radius) over a 10 μm deep sealed cavity. The shallow capacity depth provides built-in overforce protection. The diaphragm is instrumented with piezoresistors in a Wheatstone bridge configuration. Sensitivity to force is realized via the addition of a solid dome over the silicon diaphragm. The dome transmits the applied force to the diaphragm. Torlon and epoxy domes are bench tested. The epoxy dome produces significant hysteresis, while the Torlon dome shows low hysteresis (2.4% of the mean output) and low nonrepeatability ($<2.8\%$ of the mean output). The Torlon dome is subjected to a variety of loads to investigate the sensor's performance. In all cases, force accounts for at least 99.2% of the total variance in the output. Output sensitivities of 1.4 mV^{-1} N^{-1} are typical. The response is linear for low forces (<10 N) and becomes curvilinear at higher forces when the diaphragm bottoms out. The corner point between the linear and curvilinear portions of the output response can be controlled via diaphragm radius, diaphragm thickness and cavity depth. Details of the microfabrication and micromachining processes are presented along with characterization of the force-sensor system. Preliminary finger-mounted results are presented.

Keywords: Force sensors; Medicine; Robotics; Silicon; Tactile sensors

1. Introduction

Tactile sensing or taction is defined as the continuous sensing of variable contact forces [1]. Tactile sensing generally refers to a membrane with skin-like properties in which array of sensing elements measures contact stress. Harmon [2] surveyed academic researchers and industrial manufacturers to determine tactile-sensing requirements and potentials. Harmon and others [1,3,4] conclude that ideal tactile-sensing devices should contain sensors in a durable skin-like substrate, have jointed dexterous fingers and perform processing at the sensor level. Desired sensor performance characteristics include: (1) spatial resolution of 2–3 mm; (2) load range 0.1–100 N; (3) response time of 1–10 ms; (4) low hysteresis; (5) compliant and robust packaging. The specific performance requirements may vary greatly depending on the application. The performance requirements for a sensor A used in a well-defined manufacturing task may be very different from those for a sensor B used in a prosthetic device. While the environment seen by sensor A is controlled within narrowly defined limits, the environment seen by sensor B can vary greatly. The literature generally focuses on the goal of producing a tactile sensor that mimics the human sense of touch. While this may be necessary for some applications, many applications do not require such stringent requirements. Industrial applications for tactile sensors include assembly, machining, painting, sorting and stacking. Other applications include use in hazardous and/or visually obscured environments, teleoperator systems, sensory substitution systems and prosthetic systems.

1.1. Previous work

Researchers have investigated many transducing methods in the search for usable force sensors for robotics and medicine. Force sensors have been constructed based on optical, capacitive, piezoresistive, piezoelectric, ultrasonic and conductive-polymer principles. The literature contains numerous reviews of tactile-sensing technology [1,3–7]. While many methods have been investigated for used in force-sensing

applications, none has found widespread use. Each method has one or more disadvantages which make it unsuitable for nonresearch settings. These drawbacks include lack of skin-like packaging, excessive size, limited force range and lack of overforce protection. Since the design presented here is based on the piezoresistive effect in silicon, only silicon-based sensors will be discussed. Researchers have developed a plethora of silicon-based pressure sensors. Suzuki et al. developed a silicon tactile imager based on an array of capacitive cells [8]. Samaun et al. developed an early piezoresistive pressure sensor that could be catheter mounted [9]. Lee and Wise developed a silicon capacitive pressure sensor [10]. Tanigawa et al. developed a silicon pressure sensor with on-chip signal processing [11]. Wolffenbuttel et al. report a surface-micromachined tactile imaging sensor for the accurate detection of small surface details [12]. While these sensors are of interest and many contain on-chip signal processing, none is skin-like nor are they capable of withstanding large (100 N) force loadings. In addition, most sense pressure and not force. Sorab et al. developed a system for measuring fingertip forces during delivery of newborns using piezoresistive silicon force sensors that were placed on the clinician's fingertips [13]. These sensors lacked durability and were not suitable for measuring forces during manual work. Ko et al. and Neuman and Buckett developed a piezoresistive pressure sensor and tested it on human subjects [14,15]. However, the packaged sensor was not skin-like and the design was not easily adapted to producing multiple sensor arrays. Many of the attributes of silicon piezoresistive sensors are well suited to tactile sensing. Silicon has a strength comparable to that of steel with a tensile strength exceeding 689 MPa [16]. Silicon is theoretically a perfect elastic material and has no grain boundaries, which contribute to creep and hysteresis. High gage factors can be achieved. Furthermore, the sensors can be made very small. However, lead attachment, available packaging and a method of transmitting an applied force to the silicon diaphragm are problems.

One non-silicon sensor not discussed above is the conductive-polymer sensor, which is being used in several applications [17]. Conductive-polymer sensors, however, have significant hysteresis and poor accuracy [18]. They have found use mainly because of their low cost and because of the lack of a better alternative. The design proposed here attempts to overcome many of the shortcomings that have prevented other designs from finding widespread use in industrial and clinical settings. The proposed design specifically addresses the problems of appropriate packaging, overforce protection and force transmission.

2. Design, fabrication and materials

The sensor design consists of a modified silicon diaphragm structure packaged in a skin-like polyimide package. The package design is an extension of the work by Barth et al. [19] on silicon temperature sensors. A thorough discussion of the packaging materials, package fabrication and package durability is given elsewhere [20]. The sensor design is described first, followed by a discussion of the fabrication process used to build the sensor.

2.1. Sensor design

In a typical silicon piezoresistive diaphragm sensor, a cavity is etched in the silicon to form the diaphragm. Typically, the silicon is bonded to a glass substrate to form the reference chamber. Resistors are either diffused or ion implanted into the top surface of the diaphragm. Most often four resistors are used in a Wheatstone bridge configuration to increase sensitivity and minimize temperature effects on the output. The resistors are located near maximal stress points located near the edges of the diaphragm [21]. When a pressure differential exists across the diaphragm, the diaphragm deforms. The deformation changes the stress seen by the piezoresistors and their resistance changes. The changes in resistance cause a change in the bridge output voltage, which is proportional to the pressure differential. The typical diaphragm sensor is commonly used to measure gas or fluid pressures and is vulnerable to breakage from large loads. By utilizing silicon-to-silicon bonding and carefully controlling the depth of the reference chamber, a similar diaphragm structure that is intrinsically protected from breakage even at large loads can be fabricated. Such a structure has been described by others [22,23]. Although this structure is capable of withstanding large pressures without damage, it is not capable of sensing force. In order to sense force, a force-transmission structure (solid dome) must be added to distribute an applied force load over the diaphragm surface. A top and side view of the complete packaged sensor is shown in Fig. 1. Fig. 2 is a cross section showing the details of the sensing element.

The solid dome serves two purposes. First, it distributes any applied force over the surface of the diaphragm. In effect,

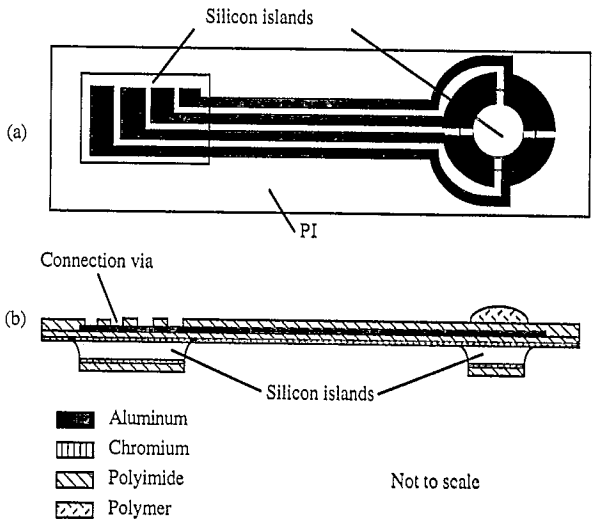

Fig. 1. The packaged sensor consists of a silicon sensing element and Al leads sandwiched between protective polyimide layers. (a) Top view and (b) side view of the complete sensor–package combination.

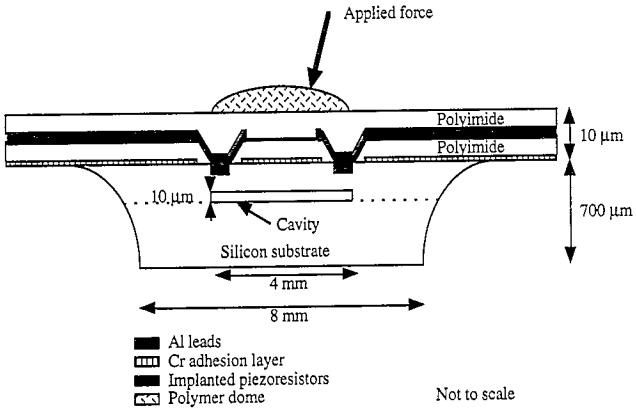

Fig. 2. The sensing element is based on a thick diaphragm structure. The applied force is transmitted to the diaphragm via a solid dome structure.

the dome is a force-to-pressure converter. Under load the diaphragm deforms, causing a corresponding change in resistor value. Secondly the dome protects the diaphragm from damage when encountering sharp objects. By an appropriate choice of diaphragm thickness, diaphragm diameter and cavity depth, the diaphragm will bottom out prior to breakage.

2.2. *Fabrication*

The flexible sensor system is realized as follows and is shown in Fig. 3(a)–(e). The process uses two wafers. The first, referred to as the sensing wafer, is a double-side polished n-type silicon wafer (⟨100⟩, more than 5 Ω cm resistivity, 200 μm thick, 3 inch diameter). The second, referred to as the substrate wafer, is a single-side polished wafer (400–500 μm thick, 3 inch diameter). To form the diaphragms, 'circular' cavities (4000 μm diameter, ≈ 10 μm deep) are etched into one side of the sensing wafer as shown in Fig. 3(a). (The 'circular' cavities are actually circular approximations limited by the original polygon mask definition and the preferential KOH etch rates. For wide shallow cavities the approximation is good.) An SiO_2 layer (1.2 μm) is grown on the wafer using a wet oxidation chamber (1000 °C for 6 h). Due to the lack of an aligner capable of double-side alignment, a manual double-side alignment jig is used to align the cavities (on one side of the wafer) to alignment marks (on the other side of the wafer). The alignment jig allows alignment of ±100 μm. While better alignment is desired, this is sufficient given the relatively large diaphragm diameter (4000 μm). These alignment marks are for resistor alignment to the diaphragm in later processing steps. The oxide is etched with BOE (buffered oxide etch, ≈0.1 μm min^{-1}). Using the oxide as a mask, the cavities and alignment marks are etched into the silicon using KOH (potassium hydroxide, 21 °C, ≈2.2 μm h^{-1}). Using BOE, the oxide on the cavity side of the wafer is removed. Next the sensing wafer is bonded to the substrate wafer using silicon fusion bonding techniques [23,24]. The wafers to be bonded are carefully cleaned in a base bath (6:1:1, H_2O:NH_4OH:H_2O_2) at 70–80 °C and hydrated in a sulfuric acid/hydrogen peroxide solution (3:1 ratio), at 80–100 °C for 5 min. After a spin dry, the polished side of the substrate wafer and the cavity side of the sensing wafer are placed together as shown in Fig. 3(b). Pressure is applied at one edge to initiate the bonding process. The bonded pair is inspected using an infrared camera (Hitachi KP-160 CCD camera). The bonded wafers are then annealed in N_2 at 1000 °C for one hour. The next step is to implant the resistors on the diaphragm. The oxide is patterned to form four resistors over each diaphragm. Two tangential and two radial resistors are used (the tangential resistors are arc shaped, the radial resistors are rectangular). The resistors are aligned to the ⟨110⟩ direction of the silicon crystal. A partial BOE etch is used to etch the oxide partially to a depth of ≈0.51 μm at the desired resistor locations. Boron is then implanted to form resistors in the silicon wafer (200 keV, dose = 2.0×10^{14}) as illustrated in Fig. 3(c).

After the sensor device or array is fabricated on the wafer, an IC (integrated circuit)-compatible process is used to fabricate the flexible package. The wafer is cleaned using a standard wafer-cleaning process and thin chromium (Cr) adhesion layer (≈100 nm) is deposited (sputtered) on both sides of the wafer. It is important that the native oxide be removed just prior to deposition for good Cr adhesion. The Cr is removed with a wet etch to expose the implemented piezoresistor regions. Next PI-2611 is spin coated on both sides of the wafer at 4000 rpm for 30 s. The polyimide (PI) is soft-baked for 30 min at 135 °C and cured for 1 h at 400 °C. This procedure yields a PI thickness of about 5 μm. The

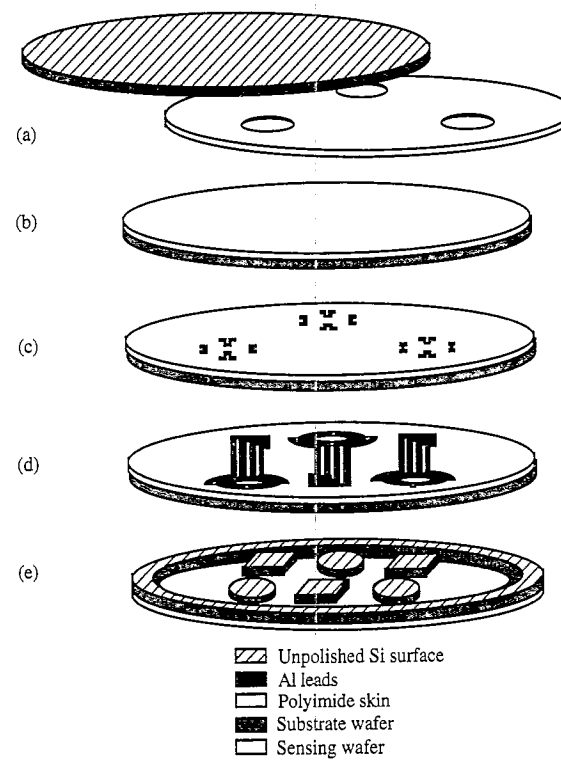

Fig. 3. The major fabrication steps include: (a) cavity formation; (b) silicon fusion bonding to form sealed reference chambers; (c) ion implantation to form the piezoresistors; (d) Al deposition and lead patterning; (e) an isotropic etch to realize individual sensors.

same spin speed and cure schedule were used for all PI layers. Vias are plasma etched in the top layer PI to allow connection to the resistor contacts. An O_2:CF_4 (50:1) plasma is used to achieve sloped side walls for improved step coverage [25]. Good adhesion at the via edges is maintained by a ring of Cr near the edge of the contact areas. The lead metal (Al) is deposited (sputtered) over the top PI layer to a thickness of 4000 Å and patterned as shown in Fig. 3(d). Aluminum was chosen as a lead metal because it is commonly available and requires no adhesion or barrier layers. Poor metal-to-PI adhesion is a well-known problem. In situ back-sputtering has been shown to improve adhesion and was used here prior to Al deposition [26]. Another layer of PI is applied over the top of the leads; thus the leads are sandwiched between protective PI layers. Next vias are etched (O_2 plasma) in the top layer PI to allow connection to the Al leads. To prepare the backside for the isotropic etch, the PI is patterned in an O_2 plasma and the underlying Cr adhesion layer is removed to form the PI/Cr isotropic etch mask. Connectors are attached to Al contact pads using a silver epoxy (EPO-TEK® H20E, 10 min cure at 150 °C). Insulating epoxy (Elmer's super-fast epoxy cement) is used to cover the connection. The insulating epoxy provides strain relief for the attached wire and protects the metal bonding area from exposure to fumes during the isotropic etch. The backside is isotropically etched in an etchant of 15% HF:85% HNO_3 as shown in Fig. 3(e). During the isotropic etch the topside is protected using a Teflon wafer holder similar to that used by King et al. [27]. Finally a razor blade is used to cut out the three identical packaged sensors produced on a single wafer.

2.3. Plastic deformation

Plastic deformation has been reported as a result of high-temperature processing [28]. A dome was observed in the diaphragms on approximately one-third of the cavities fabricated. All of the cavities appeared to be sealed via IR inspection. The domes could be caused by plastic deformation, trapped pressurized gas, residual stress or a combination of these. As discussed by Leroy and Plougonven [28], plastic deformation in silicon wafers is dependent on temperature and temperature gradient, the amount and form of precipitated oxygen and the initial wafer bow. In the case of sealed cavities, the plastic deformation of the diaphragm is also dependent on the contents trapped in the cavity, and the geometry and dimensions of the cavity [29,30]. In the bonding procedure used, the wafers were dried via spinning only. As a result, it is believed that the domed cavities appeared over cavities that contained larger amounts of trapped water. The trapped water would give rise to higher cavity pressures and at high annealing temperatures plastic deformation may result in a permanent dome shape. The sensor data reported here are from sensors with no plastic deformation present. Because the forces of interest are relatively high (up to 100 N), the effect of any residual gas in the cavity on the sensor response is minimal [31].

2.4. Force-transmission structures

In order to measure force using a pressure-sensitive device, an additional structure is required over the diaphragm so that any applied force is distributed across the diaphragm. A solid dome structure was chosen for this study. To keep the total height of the sensor small, 0.5 mm high domes with a spherical radius of 4.25 mm and a diameter of 4 mm (equal to the diaphragm diameter) were constructed out of Torlon. Torlon is a polyamide-imide that is easily machined. Similar domes were constructed using five-minute epoxy (Elmer's super-fast epoxy cement). The Torlon domes were machined, while the epoxy domes were formed simply by placing a drop of epoxy on the diaphragm. Thus the dimensions of the epoxy dome are approximate. The choice of materials was based on ease of use and difference in stiffness. The Torlon domes are attached to the diaphragm using super-glue.

3. Methods and results

To evaluate the sensor's performance, both static and dynamic loading methods are used. The sensor is tested under uniform pressure and under a variety of different-shaped load surfaces. The variance results are listed in Tables 1 and 2. Three sensor configurations/loads were tested: (1) sensing element with no force-transmission structure under a uniform pressure; (2) sensing element with an epoxy dome under different load shapes and locations; (3) sensing element with a Torlon dome under different load shapes, locations and angles. The load shapes (A, B, C, D) are illustrated in Fig. 4(a). The load locations (1, 2, 3, 4 and 5) relative to the radial and tangential resistors are shown in Fig. 4(b). Finally,

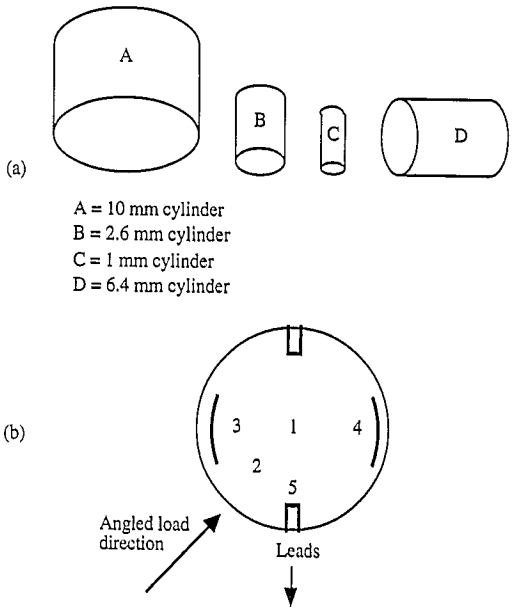

Fig. 4. The sensor was tested under a variety of load shapes, sizes, locations and angles: (a) the four loads; (b) the location of load application relative to resistor placement.

preliminary finger-mounted tests are performed using the Torlon dome as the force-transmission structure.

While traditionally pressure/force sensor performance is reported in terms of percentage of full-scale output, a statistical approach was used here with the results shown in Tables 1 and 2. A full factorial experimental design was implemented in order to study the interactions between the individual effects [32]. The design included the following factors: (1) force, (2) loading direction, (3) load shape, (4) load location and (5) load angle. The effects of varying the load shape and load location/angle were studied using analysis of variance to evaluate the differences between the means of five force levels (2, 5, 8, 11, 14 N). The F-ratio (F) is computed as the mean square (sum-of-squares divided by the degrees of freedom) divided by the mean-square error. The percentile of the F distribution (p) is used to indicate the probability of rejecting the null hypothesis when it is true, or to determined the statistical significance of the effect. Significance levels of less than 0.05 were considered statistically significant. The percentage of the variance due to a particular factor can be determined by dividing the sum of squares for each factor of interest by the total sum of squares. While a zero-load offset voltage was present, the offset voltage was subtracted from all data to reflect zero output under no-load conditions for clarity and comparison purposes.

Although the use of a Wheatstone bridge minimizes the temperature sensitivity, silicon pressure sensors still exhibit significant temperature coefficients due to tracking errors. Various compensation techniques have been used with good results [33,34]. Since the testing reported here was carried out in a controlled environment, temperature compensation was not incorporated in this work, but it will be required for future human-subject studies.

3.1. Static calibration

The static calibration tests were performed on the sensing element shown in Fig. 2. Physical limitations of the test equipment required the removal of the dome and top-layer PI. The sensor was mounted on a header and subjected to pressures using an air-drive gas compressor (Autoclave Engineers, DLE 30-1-01). The bridge output voltage was recorded manually with a digital multimeter. A reference pressure measurement was provided by a commercially available pressure sensor (Sensotec, STJE/1891-07). For each test, the load pressure was increased to approximately 500 psi. The pressure was then decreased in stepwise fashion at approximately 50 psi intervals and the bridge output voltage recorded at each level. Three repetitions were performed. A typical static calibration curve is shown in Fig. 5 with the sensor output (mV) on the y axis and the applied pressure (psi) on the x axis. Regression of the sensor output against the ten force levels below the bottoming-out point in the linear portion of the output response shows excellent linearity ($R = 1$). The sensor output becomes curvilinear at approximately 350 psi.

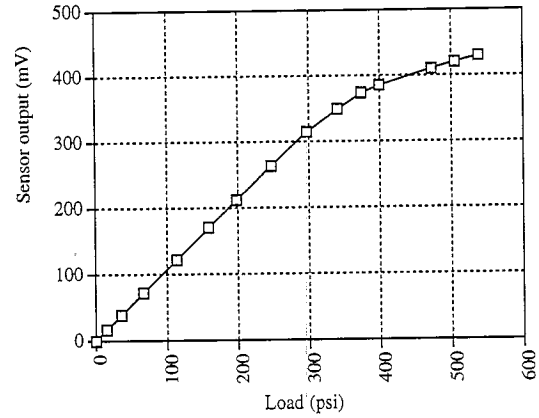

Fig. 5. A typical static calibration curve illustrates the linear and curvilinear portions of the sensor output.

3.2. Dynamic calibration methods

For dynamic testing, the sensor was placed on a rigid aluminum block and the force was applied manually using a modified drill press. A load cell (Interface, C07018/SM100) attached to the press provided an accurate measure of the actual applied loads. Various load shapes and sizes could be attached to the load cell to simulate objects encountered in daily living environments. Using this set-up, loads of known force, shape, location, angle and direction can be applied to the sensor. The load cell and sensor outputs were amplified using single operational-amplifier instrumentation amplifiers. The amplifier outputs were sampled at 30 Hz using a 12-bit analog-to-digital conversion in a Macintosh II. LabVIEW was used for data collection. The data presented in this paper were smoothed using a moving average filter. Statistical analysis for the Torlon dome data was performed using SYSTAT for data sampled at five selected force levels (2, 3, 8, 11, 14 N). A cycle consisted of applying an increasing load beyond the point where the diaphragm begins to bottom out and then decreasing the load back to zero (referred to as increasing and decreasing loading direction). The cycle was repeated three times for each load size. Typical calibration curves for both epoxy and Torlon domes are shown in Fig. 6(a, b) with the sensor output (mV) on the y axis and the applied force (N) on the x axis. Note that the output is linear for small forces (i.e., prior to the diaphragm bottoming out) and curvilinear at large forces (i.e., after the diaphragm bottoms out). The corner in the curve is the point at which the diaphragm bottoms out.

3.3. Load shape and location for the epoxy dome

The sensor output was measured while applying dynamic loads normal to the diaphragm surface using two load shapes (see Fig. 4(a), shapes B and C) and at three locations (see Fig. 4(b), locations 1, 4 and 5). The cycle defined above was used and repeated three times for both load shapes at location 1 and shape C at locations 4 and 5. The results for shape C at locations 1, 4 and 5 are shown in Fig. 6(c) with the sensor

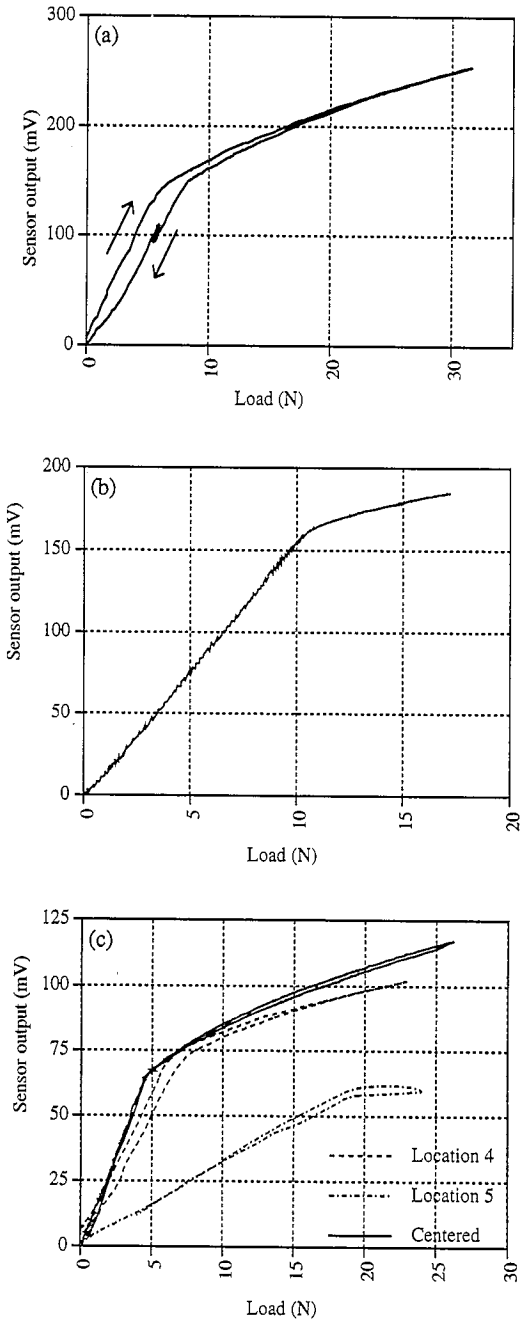

Fig. 6. (a) Under dynamic loading the epoxy dome contributes significant hysteresis to the sensor's response. (b) The use of a Torlon dome structure shows only negligible hysteresis. (c) The sensor's output is very sensitive to load location when the epoxy dome is used.

output (mV) on the y axis and the applied force (N) on the x axis. In addition, the sensor was subjected to repeated 100 N loadings with no damage.

3.3. Load shape experiment for the Torlon dome

The sensor output was measured while applying dynamic loads using four different shapes in a full-factorial experimental design (see Ref. [27] for a complete treatment of the experimental design). For each shape the load was applied centered over the diaphragm and perpendicular to the diaphragm surface. The four load shapes tested are illustrated in Fig. 4(a) and include: (A) 10 mm diameter metal cylinder, (B) 2.5 mm diameter metal cylinder, (C) 1 mm diameter metal cylinder, (D) 3.175 mm radius metal cylinder. The load shapes A, B and C were applied to the sensor with the long axis perpendicular to the diaphragm surface. Load D was applied with the long axis parallel to the surface of the diaphragm to simulate the loads seen when grasping a cylindrical object such as a pencil. The length of load shape D was much longer than the sensor width. The loading cycle defined above was used and repeated three times for each load shape. A full-factorial analysis of variance was performed as shown in Table 1. The main effects of force and direction are statistically significant ($p<0.05$), while none of the interactions is significant. The force effect accounted for 99.2% of the variance. The mean-square error term was small ($\sqrt{\text{MSE}} \approx 3.10$ mV). The error term includes variance due to nonrepeatability and systematic errors. Regression of the sensor output against the three lower force levels ($N=30$ at each force level) in the linear portion of the output response shows excellent linearity ($R=0.996$).

3.4. Load location and angle experiment for the Torlon dome

The sensor output was measured while applying dynamic loads at two locations, two angles and two directions in a full-factorial experimental design. In order to discriminate the effect of load location and angle, a small-diameter (1 mm) loading surface was used (load shape C in Fig. 4(a)). The load was applied at two locations (see Fig. 4(b), locations 1 and 3). At both locations, the load was applied at two angles (perpendicular to the diaphragm and at an angle of 10° from the perpendicular in the direction shown in Fig. 4(b)). The cycle defined above was used and repeated three times for each location/angle combination. The mean force measured at each of the five force levels used for the statistical analysis is shown in Fig. 7. As shown in Table 2, the main effects of force, location and direction are all statistically significant ($p<0.05$), as are several interactions. The force effect accounted for 99.25% of the variance. The mean-square error accounts for less than 0.07% of the variance ($\sqrt{\text{MSE}} \approx 1.8$ mV). The error term includes variance due to nonrepeatabil-

Table 1
Summary of statistical analysis for the load shape experiment

Source	Degrees of freedom	F	p
Force	4	9599	0
Direction	1	19.4	0
Shape	3	0.47	0.70
Shape × direction	3	0.23	0.88
Shape × force	12	12.27	0.25
Direction × force	4	1.17	0.33
Shape × direction	12	0.99	0.46
Error	80		

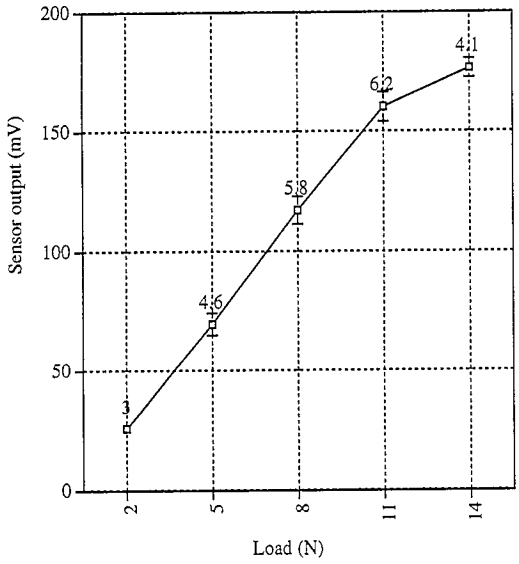

Fig. 7. The mean sensor output each force level shows good repeatability.

Table 2
Summary of statistical analysis for the load location and angle experiment

Source of variation	Degrees of freedom	F	p
Force	4	24831	0
Location	1	382.5	0
Direction	1	49.6	0
Angle	1	1.37	0.28
Location × angle	1	30.9	0
Location × direction	1	1.3	0.26
Location × force	4	22.5	0
Angle × direction	1	4.3	0.041
Angle × force	4	25.0	0
Direction × force	4	2.6	0.046
Error	68		

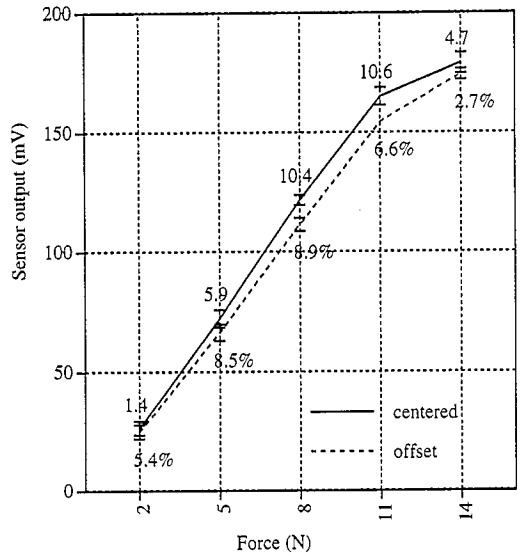

Fig. 8. The location × force interaction is significant. The difference in mean sensor output due to changes in loading location is almost 9% at the 8 N load level. Top number = difference; bottom number = percentage of mean.

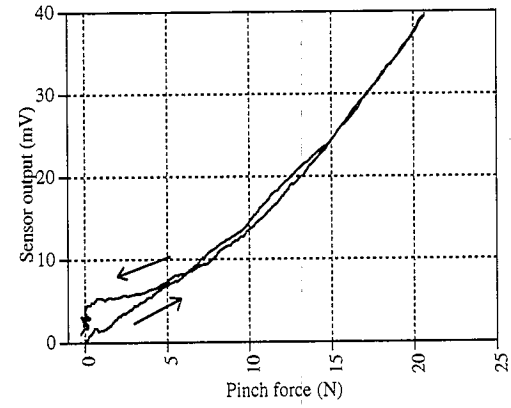

Fig. 9. A typical finger-mounted response curve shows minimal hysteresis and increased nonlinearity.

ity and systematic errors. The location × force interaction effect is shown in Fig. 8 with the sensor output (mV) on the a axis and the applied force (N) on the x axis. At each force level the top number is the absolute difference between the mean sensor outputs and the bottom number is the difference expressed as the percentage of the total mean sensor output at that force level. The errors bars show the standard deviation.

3.5. Finger-mounted tests

To evaluate the sensor's performance for medical applications and to demonstrate the advantages of the flexible package, the sensor was mounted on the thumb of a human subject and finger-mounted tests were performed. A dual-beam dynamometer was used as a reference and held between the thumb and forefinger for both tests. The dynamometer output is independent of load location along the beam [35]. The subject was instructed to increase the pinch force slowly to a predetermined level and then to release the pinch slowly. A typical response curve is shown in Fig. 9 with the sensor output (mV) on the y axis and the applied force (N) on the x axis.

4. Discussion

Robotic and medical applications for tactile sensors require that the sensor measure force accurately in a wide variety of situations. In a well-defined manufacturing grasp-and-place task the loads seen by the sensor are often highly repetitive (i.e., a single object is to be manipulated). In a teleoperator system used for hazardous waste disposal the loads may be more variable (i.e., several objects of different shapes, sizes and weights may need to be manipulated). In a force-feedback system for functional neuromuscular stimulation the sensor will see an infinitely varying array of loads just as our hands experience a wide variety of loads every day. The choice of test loads was made to test the sensor under a variety of different loads. The goal is to produce a sensor that pro-

vides the same output regardless of the load shape. Four load parameters were investigated: (1) four load shapes, (2) two loading directions, (3) two load locations, (4) two load angles. Two different force-transmission materials (five-minute epoxy, Torlon) were investigated. Finally, preliminary finger-mounted tests were performed.

Initial force load tests were performed using easy-to-construct epoxy force-transmission structures. The response curve in Fig. 6(a) shows significant hysteresis and nonlinearity, particularly on the decreasing force cycle. The nonlinear glitch on the decreasing load cycle was due to adhesion between the load surface and the epoxy dome. During decreasing load, the sudden separation of the outer ring of the load surface/dome interface causes a sudden temporary reversal in loading direction. When using a smaller load size (1 mm), the performance improves significantly in terms of linearity, hysteresis and nonrepeatability, but the output is highly dependent on load location as shown in Fig. 6(c). Overall the sensor with an epoxy dome does not show obvious improvement over the conductive polymer sensor currently used in many applications. For this reason, no further experiments were done using the epoxy dome.

In an attempt to improve the sensor's performance, new domes were constructed out of Torlon. Torlon was chosen because of its relative stiffness compared to epoxy and its ability to be machined on a lathe to form small solid domes. The sensor's performance with the Torlon dome was investigated in two experiments. The first examined the effect of load shape, while the second experiment examined the effect of load location and angle. In both experiments the effect of loading direction (increasing versus decreasing load) was also examined. Improved sensor response with the Torlon dome in terms of low hysteresis and good repeatability are illustrated in Figs. 6(b) and 7, respectively.

In the load-shape experiment, the effects of load shape, load force and loading direction were investigated. Only direction and force were found to be significant. The significance of the loading direction effect indicates that the sensor does exhibit hysteresis (i.e., the sensor's response in the direction of increasing load is different from its response in the direction of decreasing load). While the effect of loading direction is significant, its magnitude is 2.49 mV and is therefore negligible for most applications. The desirable force effect accounts for 99.2% of the total variance in the response. The effect of shape ($p=0.7$) is not significant. The mean-square error term provides a measure of repeatability. This term includes any errors not accounted for by the main effect or interactions between the main effects. These errors include variance due to nonrepeatability between repetitions and any other systematic errors. In this experiment the mean-square error term was small ($\sqrt{\text{MSE}} \approx 3.10$ mV). Thus, repeatability is very good. Regression analysis ($R=0.996$) shows that the sensor's output is linear prior to the diaphragm bottoming out. So interpreting the statistical analysis with the application in mind, the sensor with a Torlon dome shows excellent tolerance to load shape, low hysteresis, good linearity and good repeatability.

In the load location and angle experiment, the effects of load location, load angle, load force and loading direction were examined. The main effects of location, force and direction were found to be significant ($p<0.05$). In addition, several interactions were significant, but combined they account for less than 0.22% of the total variance. The effect of load location is due to the nonideal transfer of the applied force to the diaphragm. If the transfer was ideal (i.e., a point load anywhere on the dome would be transferred to the diaphragm as a uniform pressure across its surface), the output would be independent of load location. As indicated by the results, this is not true and the change in load location causes a subsequent change in the stress pattern in the diaphragm surface leading to a change in the output. While the effect of load location is significant, its magnitude is small when compared to the overall sensor output mean (4.36 mV versus 108.66 mV). The interaction effect between location and force increases with increasing load until the diaphragm bottoms out as illustrated in Fig. 8. At 8 N the difference in sensor output due to load location is 10.4 mV (8.9% of the mean sensor output) and is important. In actual use the object being manipulated is often much larger than the sensor. If the load is large in size compared to the sensor, the effect of load location is eliminated. As discussed in the previous experiment, the significance of the loading-direction effect indicates the sensor does exhibit hysteresis. Again, it is very small with an average magnitude of 2.57 mV. The effect of load force accounts for almost 99.5% of the total variance seen in the sensor's output. The small mean-square error term indicates good repeatability.

These two experiments show that the sensor's output responds largely to the magnitude of the applied force and that the effects of loading direction (hysteresis) and load location, while statistically significant, are negligible for typical applications. Repeatability and linearity are excellent, while load shape and load angle have no significant effect on the sensor's output. So for applications that allow the sensor to be mounted against a rigid substrate, the sensor is well characterized via these results. Some applications require that the sensor be mounted on less desirable substrates. For medical uses, finger mounting is often required. To examine the usefulness of this sensor in these types of applications, finger-mounted tests were performed. By pinching your fingers together and observing the skin's deformation and subsequent return to its unloaded state, it is easy to see that the human finger is less than ideal as a substrate for sensor mounting. It has hysteresis and is very nonlinear. In addition, in this experiment the subjects released their pinch and repositioned their fingers between each cycle. This will lead to increased variability, but it is similar to the way we grasp objects in everyday life (i.e., our grip varies even when grasping the same object). Thus, as expected, the performance of the sensor on the finger is degraded as compared to that of the sensor in the unmounted tests. The increase in hysteresis between

unmounted and finger-mounted results appears small, except during decreasing load (at very low force levels). The cause of this bump of hysteresis/creep is still undetermined. Future tests will attempt to pinpoint the cause. Possible causes include the additional urethane protective backing added to the sensor package for the finger-mounted tests. The other obvious change in performance is the decreased sensitivity and linearity. It is obvious that the sensor is not seeing all of the load as the output is somewhat reduced for similar loads as compared to the unmounted sensor. It is possible that at small loads some of the force bypasses the force-sensitive region (the dome) of the sensor. For example, the dome and the outer portions of the sensor may both be in contact with the dynamometer. As the load increases, more and more of it is seen by the dome and thus the sensitivity increases accordingly.

5. Conclusions

While all of the sensor characteristics desired by Harmon [2] and others [1,3,4] have not yet been achieved, significant progress is being made. The micromanufactured sensor described here has a wide load range of 0–100 N, low hysteresis, good linearity over a limited but controllable range and good repeatability. It is packaged in a durable skin-like package which can conform to a variety of surfaces. The sensor measures force magnitude accurately regardless of the load shape, location or angle. The next generation of this design will address the issues of spatial resolution and temperature compensation. Preliminary fabrication trials have shown that spatial resolutions on the order of 2–4 mm center-to-center are feasible. The finger-mounted tests illustrate the advantages of the flexible packaging. Simple changes in the mask set will yield a flexible array of smaller force sensors. Such a tactile skin can then be used to cover a robotic manipulator regardless of shape. As discussed above, there is a wide variety of applications for tactile sensors, each application having its own unique set of sensor requirements. By changing the physical parameters of the design (diaphragm thickness, diaphragm diameter, cavity depth), the sensor's characteristics can be tailored to the application. Fig. 10 illustrates the tradeoffs between diaphragm thickness, diaphragm diameter and cavity depth.

Future work includes finite-element modeling of various dome materials and shapes, additional finger-mounted tests and statistical analysis, further optimization of package durability and the fabrication of closely spaced arrays with on-chip temperature compensation.

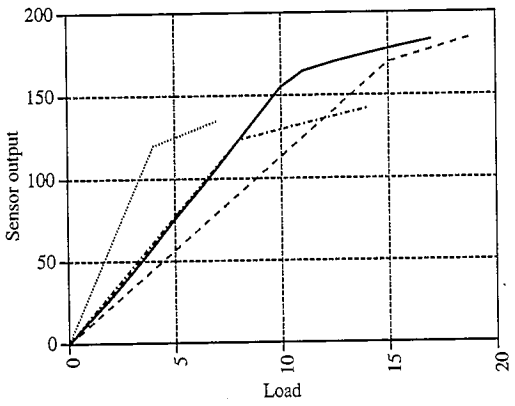

Fig. 10. By changing the physical parameters of the sensing element, the performance characteristics can be tailored to meet the requirements of specific applications: solid line, prototype; dotted line, decreasing diaphragm thickness and/or increasing diameter; dashed line, increasing diaphragm thickness and/or decreasing diameter; dash–dot line, decreasing cavity depth.

Acknowledgements

The authors would like to thank Dan Christensen, and Professor John G. Webster for many helpful discussions. Thanks to Kevin Cohen for his help with data acquisition. David Beebe was supported by NIH Grant 5T32GMO8349. We are grateful to DuPont for providing all polyimides used in this work. We are grateful to SSI, Inc. (Mike Mattes and Jim Seefeldt) for the use of their high-pressure vessel for the static calibration tests. Thanks to Professors Webster and Tompkins for the use of their data-acquisition equipment.

References

[1] K.E. Pennywitt, Robotic tactile sensing, *Byte, 11* (1986) 177–200.
[2] L.D. Harmon, Automated tactile sensing, *Int. J. Robotics Res., 1* (1982) 3–32.
[3] P. Dario and D.D. Rossi, Tactile sensors and the gripping challenge, *IEEE Spectrum,* (1985) 46–52.
[4] J.G. Webster (ed.), *Tactile Sensors for Robotics and Medicine,* John Wiley, New York, 1988.
[5] P.P.L. Regtien, Tactile imaging, *Sensors and Actuators A, 31* (1992) 83–89.
[6] P. Dario, Tactile sensing: technology and applications, *Sensors and Actuators A, 25–27* (1991) 251–256.
[7] M. Ogorek, Tactile sensors, *Manufact. Eng.,* (Feb.) (1985) 69–77.
[8] K. Suzuki, K. Najafi and K.D. Wise, A 1024-element high-performance silicon tactile imager, *IEEE Trans. Electron Devices, 37* (1990) 1852–1859.
[9] Samaun, K.D. Wise and J.B. Angell, An IC piezoresistive pressure sensor for biomedical instrumentation, *IEEE Trans. Biomed. Eng., BME-20* (1973) 101–109.
[10] Y.S. Lee and K.D. Wise, A batch-fabricated silicon capacitive pressure transducer with low temperature sensitivity, *IEEE Trans. Electron Devices, ED-29* (1982) 42–48.
[11] H. Tanigawa, T. Ishihara, M. Hirata and K. Suzuki, MOS integrated silicon pressure sensor, *IEEE Trans. Electron Devices, ED-32* (1985) 1191–1195.
[12] M.R. Wolffenbuttel, Y.X. Li, D. Poenar, P.J. French, P.P.L. Regtien and R.F. Wolffenbuttel, Multilayer membranes for a tactile imaging sensor, using surface micromachining and RIE, *Proc. 7th Int. Conf. Solid-State Sensors and Actuators (Transducers '93), Yokohama, Japan, 7–10 June, 1993,* pp. 284–287.
[13] J. Sorab, R.H. Allen and B. Gonik, Tactile sensory monitoring of clinician-applied forces during delivery of newborns, *IEEE Trans. Biomed. Eng., BME-35* (1988) 1090–1093.

[14] W.H. Ko, J. Hynecek and S.F. Boettcher, Development of a miniature pressure transducer for biomedical applications, *IEEE Trans. Electron Devices, ED-26* (1979) 1896–1905.
[15] M.R. Neuman and J.R. Buckett, Thumb force and position sensors, *Proc. 35th Ann. Conf. Eng. Med. Biol., Philadelphia, PA, USA, 22–24 September, 1982,* Vol. 24, p. 122.
[16] K.E. Petersen, Silicon as a mechanical material, *Proc. IEEE, 70* (1982) 420–457.
[17] T.R. Jensen, R.G. Radwin and J.G. Webster, A conductive polymer sensor for measuring external forces, *J. Biomech., 24* (1991) 851–858.
[18] R.A. Pax, J.G. Webster and R.G. Radwin, A pressure sensing glove using conductive polymer pressure sensors, *MS Thesis,* University of Wisconsin-Madison (1989).
[19] P.W. Barth, S.L. Bernard and J.B. Angell, Flexible circuit and sensor arrays fabricated by monolithic silicon technology, *IEEE Trans. Electron Devices, ED-32* (1985) 1202–1205.
[20] D.J. Beebe and D.D. Denton, A flexible polyimide-based package for silicon sensors, *Sensors and Actuators A, 44* (1994) 57–64.
[21] S.K. Clark and K.D. Wise, Pressure sensitivity in anisotropically etched thin-diaphragm pressure sensors, *IEEE Trans. Electron Devices, ED-26* (1979) 1887–1896.
[22] Y. Wang, L. Liu, X. Zheng and Z. Li, A novel pressure sensor structure for integrated sensors, *Sensors and Actuators, A21–A23* (1990) 62–64.
[23] K. Petersen, P. Barth, J. Poydock, J. Brown, J. Mallon and J. Bryzek, Silicon fusion bonding for pressure sensors, *Tech. Digest, IEEE Solid-State Sensor Workshop, Hilton Head Island, SC, USA, 6–9 June, 1988,* pp. 144–147.
[24] M. Shimbo, K. Furukawa, K. Fukuda and K. Tanzawa, Silicon-to-silicon direct bonding method, *J. Appl. Phys., 60* (1986) 2987–2989.
[25] M. Deschler and P. Balk, Optimization of via hole plasma etching in polyimide for overlay interconnections, *Microelectron. Eng., 4* (1986) 207–219.
[26] M.J. Vasile and B.J. Bachman, Aluminum deposition on polyimides: the effect of in situ ion bombardment, *J. Vac. Sci. Technol., A7* (1989) 2992–2997.
[27] J.T. Kung, A.N. Karanicolas and Hae-Seung Lee, A compact, inexpensive apparatus for one-side etching in KOH and HF, *Sensors and Actuators A, 29* (1991) 209–215.
[28] B. Leroy and C. Plougonven, Warpage of silicon wafers, *J. Electrochem. Soc., 127* (1980) 961–970.
[29] M.A. Huff, M.S. Mettner, T.A. Lober and M.A. Schmidt, A pressure-balanced electrostatically-actuated microvalve, *Solid-State Sensor and Actuator Workshop, Hilton Head, SC, USA, 1990,* pp. 123–127.
[30] M.A. Huff, personal communication, 1995.
[31] J. Garvey, D.J. Beebe and D.D. Denton, Finite element modelling of a silicon tactile sensor, *Sensors Mater.,* submitted for publication.
[32] G.E. Box, W.G. Hunter and J.S. Hunter, *Statistics for Experimenters,* John Wiley, New York, 1978.
[33] D. Tandeske, *Pressure Sensors: Selection and Application,* Marcel Dekker, New York, 1991.
[34] M. Akbar and M.A. Shanblatt, Temperature compensation of piezoresistive pressure sensors, *Sensors and Actuators A, 33* (1992) 155–162.
[35] R.G. Radwin, G.P. Masters and F.W. Lupton, A linear force-summing hand dynamometer independent of point of application, *Appl. Ergonomics, 22* (1991) 339–343.

Biographies

David J. Beebe is an assistant professor in the Department of Biomedical Engineering and a faculty research associate in the Institute for Micromanufacturing at Louisiana Tech University. He received B.S. (1987), M.S. (1990) and Ph.D. (1994) degrees in electrical engineering from the University of Wisconsin-Madison. David was an electrical engineer for Kimberly-Clark Corp. from 1987 to 1989. From 1991 to 1994 he was an NIH biotechnology predoctoral trainee. During the summer of 1992, he worked at Medtronic, Inc. in Minneapolis, MN and developed new hemodynamic sensing concepts. He is a contributing author to W.J. Tompkins (ed.), *Biomedical Digital Signal Processing* (Prentice Hall, Englewood Cliffs, 1993) and to J.G. Webster (ed.), *Prevention of Pressure Sores* (Adam Hilger, Bristol, UK, 1991). David has broad interests in biomedical instrumentation and the development of microfabricated devices for biomedical applications. His current interests include technology development for the labeling of biological objects, development of MEMS-based tactors, development of electrostatic haptic displays and continued work on tactile sensors.

Arthur Hsieh received the BSEE degree from the University of Wisconsin-Madison in 1994. He is currently a graduate student in the Department of Biomedical Engineering at the University of Southern California.

Denice D. Denton is a professor in the Department of Electrical and Computer Engineering at the University of Wisconsin-Madison. She spent the Fall Semester of 1991 as a visiting scientist and the summer of 1993 as a visiting professor at the Swiss Federal Institute of Technology (ETH) in Zurich, Switzerland. She received B.S., M.S. (1982) and Ph.D. (1987) degrees in electrical engineering from MIT. Her current interests include the design of an integrated 'smart' moisture sensor, the investigation of the long-term reliability implications of the use of polymers in integrated circuit applications, and the use of micromachining in solid-state actuator design. Professor Denton heads the Plasma Deposition and Polymerization Thrust Area of the NSF Engineering Research Center (ERC) for Plasma-Aided Manufacturing at the University of Wisconsin-Madison. Her work in the ERC focuses on plasma deposition of polymers used in photonics applications. She is a member of the National Research Council Plasma Processing and Processing Science Panel. She is the recipient of the American Society of Engineering Education AT&T Foundation Teaching Award (1991) and the Eta Kappa Nu C. Holmes MacDonald Distinguished Young Electrical Engineering Teaching Award (1993). She is a member of the National Academy of Sciences/National Research Council Board on Engineering Education (1991–1995).

Robert G. Radwin is an associate professor in the Department of Industrial Engineering at the University of Wisconsin-Madison, where he conducts research and teaches in the areas of ergonomics, human factors and biomedical engineering. Dr Radwin has a B.S.E. in electrical engineering from the Polytechnic Institute of New York, and M.S. degrees in electrical engineering and bioengineering from the Uni-

versity of Michigan. He earned his Ph.D. in industrial and operations engineering at the University of Michigan and he was a postdoctoral research fellow at the Center for Ergonomics. He is the recipient of a Presidential Young Investigator Award from the National Science Foundation, and a Special Emphasis Research Career Award from the National Institute for Occupational Safety and Health. Dr Radwin is actively studying the causes and prevention of musculoskeletal disorders in manual work. At the University of Wisconsin-Madison he is developing electronic instruments and analytical methods for measuring and assessing exposure to physical stress in the workplace, including repetitive motion, forceful exertions, contact stress, postural stress, cold temperatures and vibration. He is also developing ergonomics guidelines for the design and use of hand-operated equipment and power tools and is investigating manual performance deficits associated with cumulative trauma disorders and peripheral neuropathies.